ACS Combinatorial Science

Research Article

pubs.acs.org/acscombsci

Temperature-Programmed Technique Accompanied with High-Throughput Methodology for Rapidly Searching the Optimal Operating Temperature of MOX Gas Sensors

Guozhu Zhang, Changsheng Xie,* Shunping Zhang, Jianwei Zhao, Tao Lei, and Dawen Zeng

State Key Laboratory of Materials Processing and Die & Mould Technology, Nanomaterials and Smart Sensors Research Laboratory (NSSRL), Department of Materials Science and Engineering, Huazhong University of Science and Technology, Wuhan 430074, PR China

Supporting Information

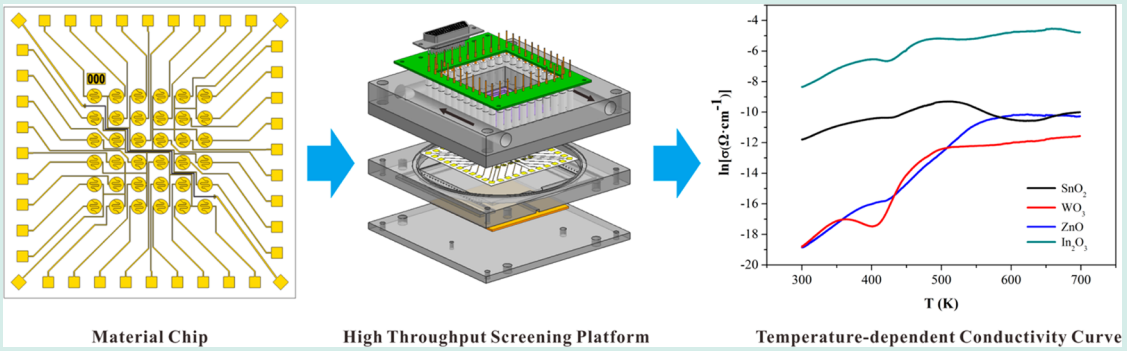

ABSTRACT: A combinatorial high-throughput temperature-programmed method to obtain the optimal operating temperature (OOT) of gas sensor materials is demonstrated here for the first time. A material library consisting of SnO_2, ZnO, WO_3, and In_2O_3 sensor films was fabricated by screen printing. Temperature-dependent conductivity curves were obtained by scanning this gas sensor library from 300 to 700 K in different atmospheres (dry air, formaldehyde, carbon monoxide, nitrogen dioxide, toluene and ammonia), giving the OOT of each sensor formulation as a function of the carrier and analyte gases. A comparative study of the temperature-programmed method and a conventional method showed good agreement in measured OOT.

KEYWORDS: *high-throughput screening, gas sensor, arrays, temperature-dependent conductivity, isothermal technique, oxide materials*

INTRODUCTION

Ever since combinatorial methods were applied to materials science,[1] high-throughput techniques have become widely used in the discovery of novel electronic,[2] magnetic,[3] and optical materials.[4,5] Many high-throughput applications have been developed for gas-sensing materials, including sensors to detect toxic and pollutant gases.[6] For example, Semancik et al. employed 36-element sensor arrays to evaluate various surface-dispersed catalytic additives on equivalent CVD SnO_2 films.[7] Simon and co-workers used high-throughput impedance spectroscopy to characterize and screen sensing materials loaded in 64 multielectrode arrays.[8−10] A previous study from our laboratory employed a high-throughput screening platform of gas sensing materials (HTSP-GM) to rapidly screen functional metal oxide (MOX) semiconductor gas sensors.[11] While most of these efforts have focused on the evaluation of the gas sensitivity and selectivity, the optimal operating temperature (OOT) is also as an important performance parameter for the gas sensors. OOT determines the power consumption and other gas-sensing characteristics, including reliability and durability of the gas sensors.[12]

OOT is usually determined with performance tests at different temperatures, inferring the optimum temperature of each gas sensor individually,[13−15] which is time-consuming and inefficient. To address these difficulties, we describe here a temperature-programmed measurement technique which gives more information in much less time.

Temperature-programmed techniques are often used in applied surface science and catalysis, with different applications such as temperature-programmed desorption (TPD),[16] temperature-programmed reaction (TPR),[17] thermogravimetric analysis (TGA),[18] and differential scanning calorimetry (DSC).[19] With these measurements, one can acquire physical and chemical parameters dynamically and explore their interdependence in the material. For MOX sensor materials, the adsorption and desorption of gases causes changes in electrical conductivity of semiconductor[20] in a temperature-dependent and atmosphere-dependent manner.[21−23] The OOT of the MOX is the temperature at which the maximum conductivity difference is observed between the target gas and carrier gas. To our best knowledge, temperature-programmed techniques have not been

Received: November 23, 2013
Revised: May 14, 2014
Published: August 4, 2014

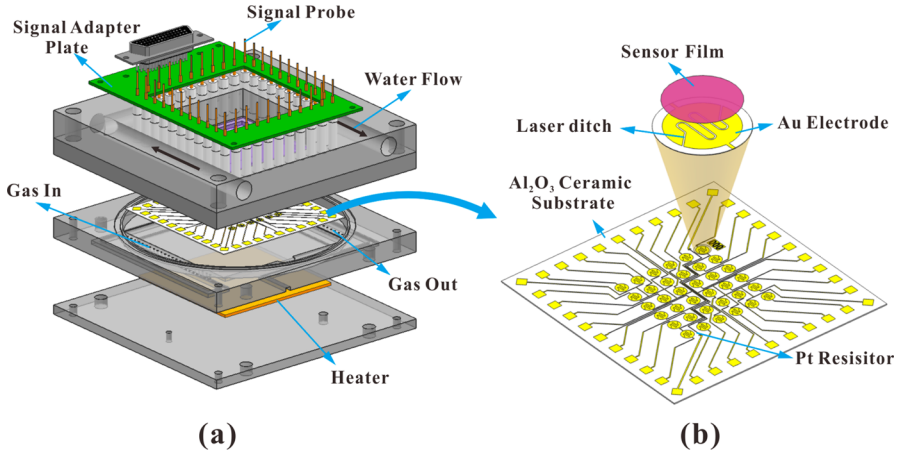

Figure 1. (a) Schematic illustrations of test chamber of high-throughput screening platform of gas-sensing materials (HTSP-GM). (b) Schematic layout of 36-matrices material chip.

applied to the determination of OOT values in MOX materials so far.

Our approach to this problem integrates temperature-programmed measurements with a high-throughput screening platform of the gas sensing materials (HTSP-GM). In this study, SnO_2, ZnO, WO_3 and In_2O_3 sensor materials are loaded in a 36-position chip array,[11] followed by temperature-programmed tests in carrier gas and different atmospheres. The OOT can be obtained from the difference value of the resulting temperature-dependent conductivity curves. This simple but powerful analytical method was compared to the standard isothermal test, with promising results.

EXPERIMENTAL PROCEDURE

Sample and Device Preparation. Metal oxide materials exhibit many advantages for gas sensing, including high sensing performance, easy fabrication, low production cost, and promising realistic applications. Among these materials, SnO_2, WO_3, ZnO, and In_2O_3 based gas sensors have received substantial attention,[24−27] and so were chosen for this investigation. Nanosized SnO_2 was synthesized by a simple hydrothermal route.[24] WO_3 was synthesized by an infiltration and calcination process using cotton fiber as template which has been reported previously by us.[25] ZnO and In_2O_3 were prepared by homogeneous precipitation[26] and sol−gel formation,[27] respectively. Afterward, pastes were obtained by mixing oxide powders with organic solvent in an agate mortar. These preparations were then applied to a screen printing technique for preparing thick films on a 36-sample flat material matrix chip, as shown in Figure 1b. The resulting chip was transferred to the test chamber (Figure 1a) for aging. Details concerning the specific materials composition and device fabrication processes are presented in the Supporting Information.

Fabrication of the Measurement Platform. Figure 2 showed the test platform,[11] consisting of five components, including the computer, the data control module, gas flow rate control module, temperature control module, and the test chamber. The temperature controller (SDC35, Azbil Co., Japan), establishes working temperatures from room temperature to 500 °C with sensitivity better than ±0.1 °C. For temperature testing and feedback, a Pt resistor was printed on the material chip, as shown in Figure 1b. The testing resistance range of the platform is $10-10^8$ Ω within an error of 5%.

Measurement Processes of the Temperature-Programmed Test and Conventional Isothermal Test. In the experiment, we selected five main air pollution gases for testing, including formaldehyde (20 ppm), carbon monoxide (1000 ppm), nitrogen dioxide (0.5 ppm), toluene (20 ppm), and ammonia (100 ppm) and dry air as the carrier gas. The $R-T$ curves of the sensor films in different atmospheres were obtained at a heating rate β of 10 K/min under a flow rate of 1000 mL/min

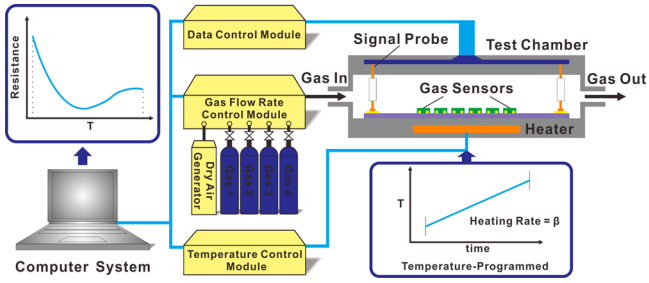

Figure 2. Scheme of high-throughput screening platform of gas-sensing materials (HTSP-GM) integrated with temperature-programmed system.

of the test gas over a temperature range of 300−700 K. For comparison, OOT values were also determined by a conventional isothermal test over the same temperature range and flow rate in steps of 50 K.

The observed $R-T$ curves were converted to ln $\sigma-T$ according to eq 1

$$R = \frac{1}{\sigma} \bullet \frac{L}{S} \tag{1}$$

where R is the resistance of the sensor film, σ is the electrical conductivity of the sensor film, L the length of the positive and negative electrode, that is, the width of the laser ditch, S is the conduction area of the sensor film. The definitions of terms for gas response using the temperature-programmed and conventional isothermal methods are given in Table 1.

Table 1. Definitions of the Sensing Response between the Temperature-Programmed Test and Conventional Isothermal Test[a]

gas category	temperature-programmed test	isothermal test
reducing gas	$S(T) = \exp[\ln \sigma_{air}(T) - \ln \sigma_{gas}(T)]$	$S^* = \frac{R_{air}}{R_{gas}}$
oxidizing gas	$S(T) = \exp[\ln \sigma_{gas}(T) - \ln \sigma_{air}(T)]$	$S^* = \frac{R_{gas}}{R_{air}}$

[a]Notes: (1) R_{air} is the resistance in atmospheric air, and R_{gas} is the resistance of the sensor materials exposed in the target test gases. (2) Because of the existence of the measurement error of this platform, the value of $S(T)$ was set as 1 as $[\ln \sigma_{air}(T) - \ln \sigma_{gas}(T)] < 0$ or $[\ln \sigma_{gas}(T) - \ln \sigma_{air}(T)] < 0$ at a given temperature. (3) According to the formula (1), the value of S^* was equal to S, that is, $S^* = S$.

dx.doi.org/10.1021/co500054r | ACS Comb. Sci. 2014, 16, 459−465

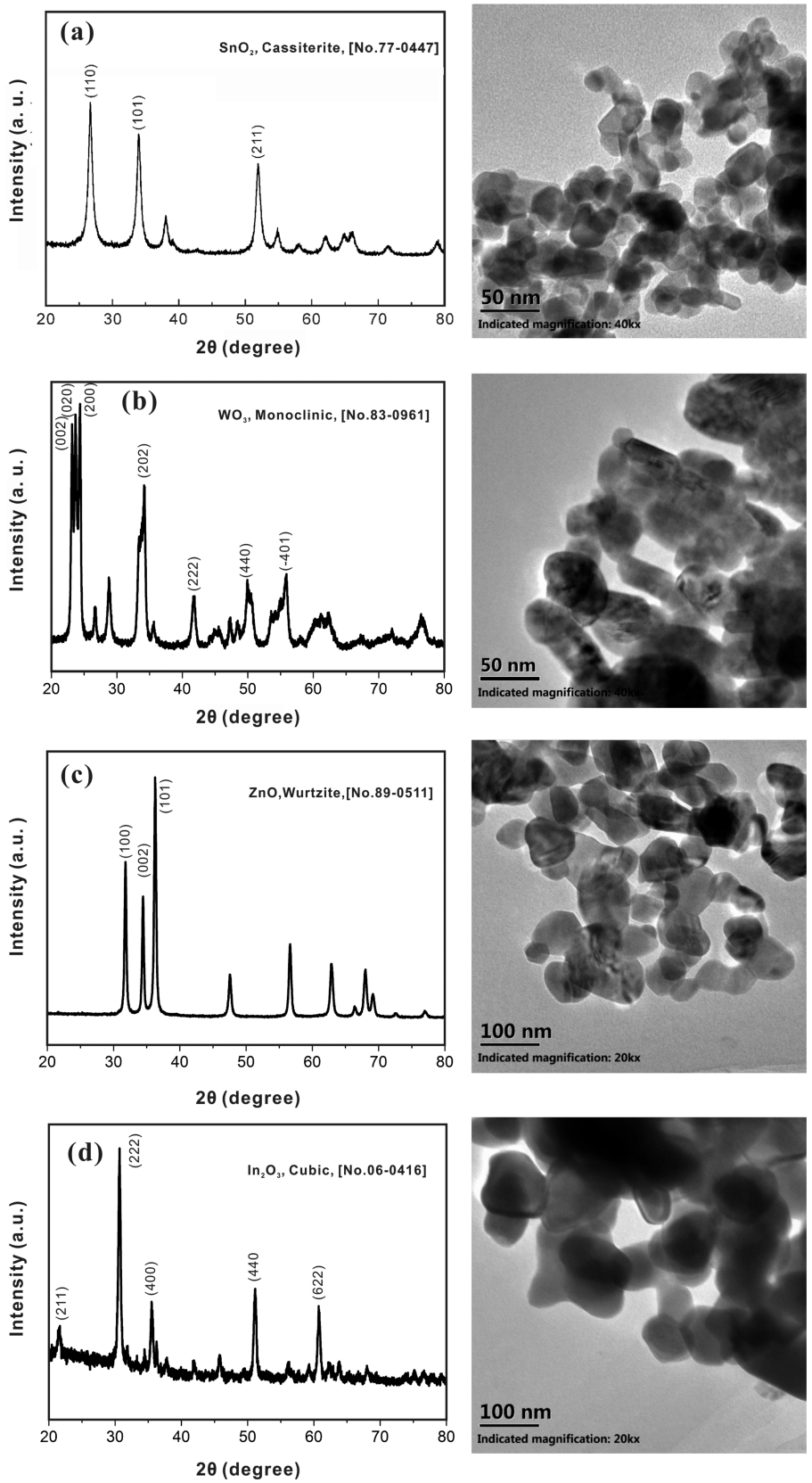

Figure 3. XRD patterns and TEM images of (a) SnO_2 nanoparticles, (b) WO_3 nanoparticles, (c) ZnO nanoparticles, and (d) In_2O_3 nanoparticles of the sensor films sintered at 600 °C for 2 h in air.

dx.doi.org/10.1021/co500054r | *ACS Comb. Sci.* 2014, 16, 459−465

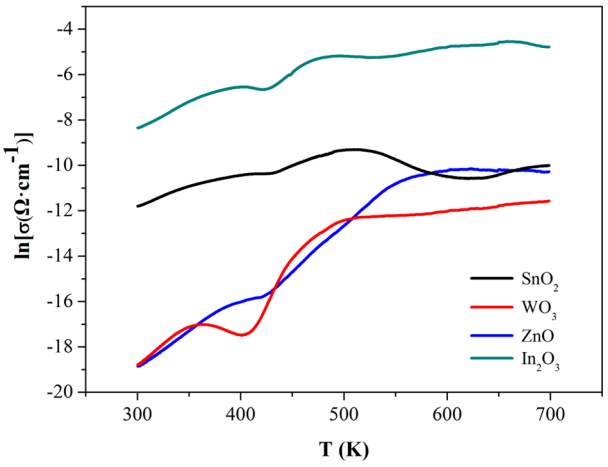

Figure 4. Typical temperature-dependent conductivity curves of SnO_2, WO_3, In_2O_3, and ZnO film in dry air with a heating rate of 10 K/min.

RESULTS AND DISCUSSION

Structure Characterization. As shown in Figure 3, the as-synthesized SnO_2, ZnO, WO_3, and In_2O_3 sensor films after calcinating for 2 h at 600 °C were characterized by X-ray diffraction (XRD) and transmission electron micrograph (TEM). The XRD patterns were consistent with indexing to tetragonal SnO_2 (JCPDS 77-0447), monoclinic WO_3 (JCPDS 83-0961), wurtzite ZnO (JCPDS 89-0511), and cubic In_2O_3 (JCPDS 06-0416), respectively. Examination of more detailed microstructures by TEM (Figure 3) showed uniform SnO_2, ZnO, WO_3, and In_2O_3 nanoparticles with an average diameter of about 20, 40, 50, and 60 nm, respectively, consistent with XRD measurements.

Typical Integrated Temperature-Programmed Testing Curve. Figure 4 shows the conductivity−temperature HTSP-GM testing curve of the four sensor films in dry air. These four materials display different conductivity properties. For SnO_2, the temperature-dependent conductivity shows a typical sigmoid behavior, as previously noted in a related study.[23,28] Two-phase behavior was observed with a slow increase in conductivity from 300 to approximately 400 K and a more rapid rise from 435 to 500 K. Conductivity fell with heating to higher temperatures. A similar type of profile was exhibited by In_2O_3 (300 to ∼400 K and ∼435−470 K). However, this oxide showed a further slow increase in conductivity at higher temperatures, with a peak reached at ∼665 K. ZnO also showed two distinct regions of increasing conductivity (from 300 to ∼575 K), while WO_3 showed three phases in the temperature range of 300−485 K. For these wide band gap semiconductors, it is expected that sintering in air destroys the synthetic metal−oxygen stoichiometry and forms oxygen vacancies.[29−32] Thus, conduction electrons mainly come

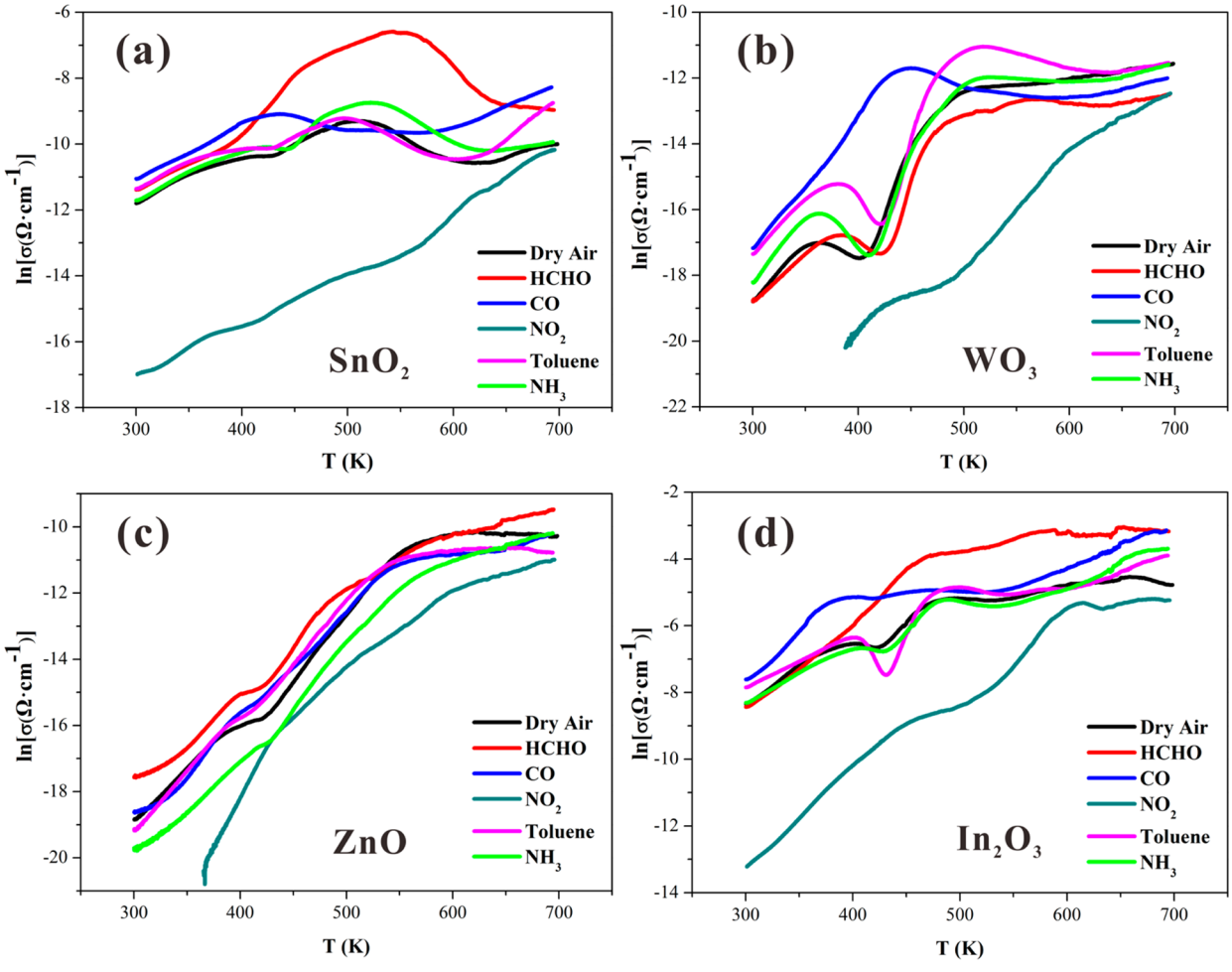

Figure 5. Temperature-dependent conductivity of the sensor films (a) SnO_2, (b) WO_3, (c) ZnO, and (d) In_2O_3 in different atmospheres with a heating rate of 10 K/min.

dx.doi.org/10.1021/co500054r | ACS Comb. Sci. 2014, 16, 459−465

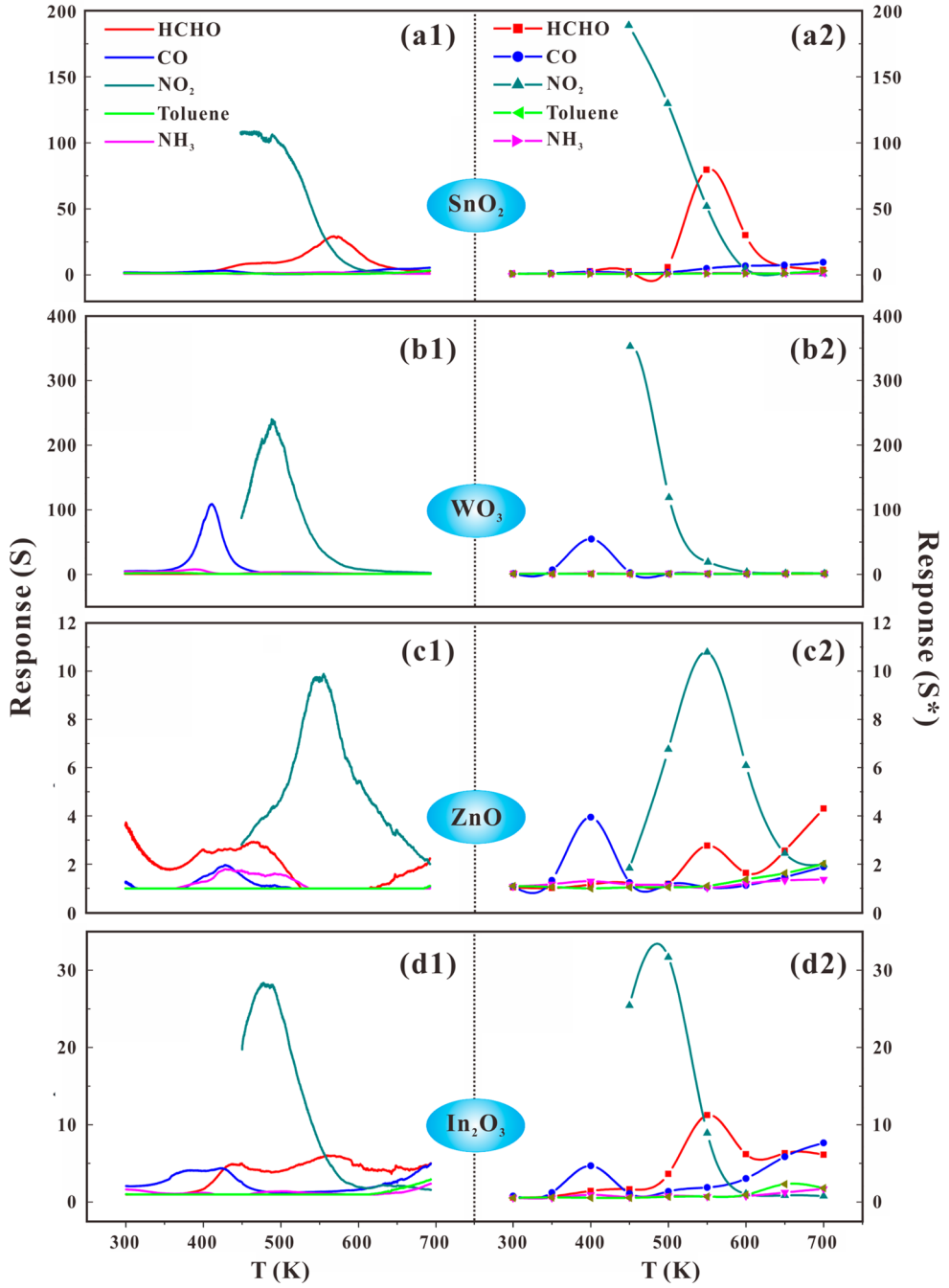

Figure 6. Comparative investigation of the optimal operating temperature (OOT) of SnO_2, WO_3, ZnO, and In_2O_3 sensor films between the temperature-programmed test (a1, b1, c1, and d1) and the isothermal test (a2, b2, c2, and d2).

Table 2. Optimal Operating Temperature (OOT) of the Sensing Materials toward Different Gases

sensing material	HCHO (20 ppm) (K)	CO (1000 ppm) (K)	NO_2 (0.6 ppm) (K)	toluene (20 ppm) (K)	NH_3 (100 ppm) (K)
SnO_2	575	427, 690	450	*a*	*a*
WO_3	*a*	412	491	*a*	393
ZnO	*a*	430	556	*a*	*a*
In_2O_3	561	425, 700	489	*a*	*a*

[a]Gas sensor was insensitive toward the gas.

from the ionization of these oxygen vacancies at such relatively low temperatures. After these defects have been fully ionized, intrinsic ionization (valence band to conductance band) is believed to be responsible to the conductivity change of these MOX materials. The sharp increase in conductivities of ZnO and WO_3 in the temperature range of 300−700 K as compared with SnO_2 and In2O_3 likely results from the formation of more impurities in the former[29,30] than that in the latter.[31,32]

Comparison of Temperature-Programmed and Isothermal Tests. Using the test procedure described above, we obtained the temperature-dependent conductivity curves of each sensor film in atmospheres of formaldehyde, carbon monoxide, nitrogen dioxide, toluene and ammonia. As shown in Figure 5, these curves exhibited remarkable differences for SnO_2, WO_3 and In_2O_3, while no obvious conductivity distinction was observed for ZnO. Formaldehyde, carbon monoxide, toluene and ammonia

dx.doi.org/10.1021/co500054r | ACS Comb. Sci. 2014, 16, 459−465

Table 3. Comparative Results of Optimal Operating Temperature (OOT) between the Isothermal Method (IS) and Temperature-Programmed Method (TP)

	HCHO		CO		NO_2		toluene		NH_3	
sensing material	IS	TP	IS	TP	IS	TP	IS	TP	IS	TP
SnO_2	~550K	575K	~400K	427K	~450K	450K	*a*		*a*	
			~700K	690K						
WO_3	*a*		~400K	412K	~450K	491K	*a*		*a*	393K
ZnO	*a*		~400K	430K	~550K	556K	*a*		*a*	
In_2O_3	~550K	561K	~400K	425K	~480K	489K	*a*		*a*	
			~700K	700K						

[a]Gas sensor was insensitive toward the gas.

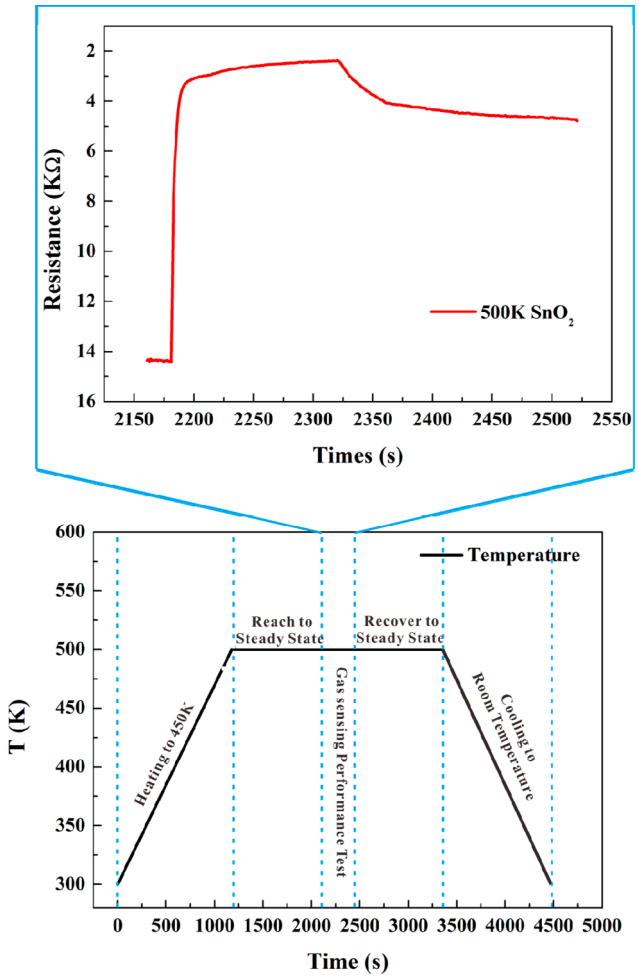

Figure 7. Time needed for the conventional isothermal sensing performance test of SnO_2 at each temperature, take formaldehyde sensing performance test at 500 K as an example.

are reducing gases, resulting in a decrease of the film resistance during gas exposure, while nitrogen dioxide is an oxidizing gas leading to the opposite behavior. On the basis of the definition of the gas response in Table 1, each sensor gives a strongest response to 0.5 ppm of NO_2 as compared with the other gases. Indeed, the resistance of WO_3 and ZnO in 0.5 ppm of NO_2 exceeds the upper limit of the platform's dynamic range, so these materials were analyzed from 390 to 700 K and 370 to 700 K, respectively.

According to the definition of the gas response for the temperature-programmed method, we get the temperature-dependent response $S(T)$ by comparing the conductivity differences in target gases and dry air. The relationship between the response and temperature $S(T)-T$ is presented in Figure 6 (a1, b1, c1, and d1). From this figure, the OOT values of these four sensors toward different gases were derived and are listed in Table 2. Again, because of the large response toward NO_2 at low temperature, the temperature-dependent response $S(T)$ was processed for this gas starting at 450 K to eliminate the test error as much as possible.

For comparison, Figure 6a2, b2, c2, and d2 also shows the gas response of each sensor at different temperatures obtained through a conventional isothermal method. While the overall results were in good agreement (Table 3; note for example that reducing and oxidizing gases induced opposite changes in resistance in both methods), the time required for acquisition of the data under isothermal conditions was far longer. For example, determination of formaldehyde at 500 K takes about 75 min, as shown in Figure 7. Thus, approximately 11.25 h (1.25 h × 9) are needed for the entire matrix at nine different temperatures. (For consistency, nitrogen dioxide was analyzed in the conventional isothermal test over a temperature range of 450 to 700 K.) Additional details for the acquisition of OOT values through these two methods are presented in the Supporting Information.

Two advantages can be concluded for the temperature-programmed method. (1) The isothermal method can only give an approximate temperature range of the OOT, while the temperature-programmed method is capable of accurately obtaining the OOT of these gas sensors. (2) The temperature-programmed method needs only 40 min or less rather than many hours (11.25 h) for the isothermal method.

In addition to the rapid determination of OOT, the temperature-programmed test can also be used for determining gas selectivity. Figure 6 (a1, b1, c1 and d1) shows good response toward nitrogen dioxide for all sensors (WO_3 giving the greatest values) and good selectivity for SnO_2 toward formaldehyde, WO_3 toward carbon monoxide, and In_2O_3 toward carbon monoxide and formaldehyde. Besides, the acquired gas responses of the sensors through temperature-programmed method are lower than the isothermal method, probably because of the dynamic and nonequilibrium nature of the temperature-dependent process, but this does not affect the searching of the OOT.

CONCLUSIONS

In this study, a HTSP-GM platform integrated with a temperature-programmed system was utilized to measure temperature-dependent conductivity curves in different atmospheres for various MOX gas sensor materials. The OOT of SnO_2, ZnO, WO_3, and In_2O_3 sensors were determined with greater precision and in far less time than independent measurements using a conventional isothermal method. Thus, high-throughput temperature-programmed analysis should be considered for the determination of OOT values in other gas sensors as well.

dx.doi.org/10.1021/co500054r | ACS Comb. Sci. 2014, 16, 459−465

■ ASSOCIATED CONTENT

Supporting Information

Experimental section and specific process of the comparative investigation of the OOT between temperature-programmed test and isothermal test by HTSP-GM. This material is available free of charge via the Internet at http://pubs.acs.org.

■ AUTHOR INFORMATION

Corresponding Author

*Tel.: +86-27-8755-6544. Fax: +86-27-87543778. E-mail: csxie@mail.hust.edu.cn.

Notes

The authors declare no competing financial interest.

■ ACKNOWLEDGMENTS

This work was supported by Nature Science Foundation of China (Nos. 51204072 and 50927201), the National Basic Research Program of China (Grant Nos. 2009CB939705 and 2009CB939702). The authors are also grateful to Analytical and Testing Center of Huazhong University of Science and Technology.

■ REFERENCES

(1) Xiang, X. D.; Sun, X.; Briceno, G.; Lou, Y.; Wang, K.; Chang, H.; Wallace-Freedman, W. G.; Chen, S.; Schultz, P. G. A Combinatorial Approach to Materials Discovery. *Science* **1995**, 1738−1738.

(2) Leugers, A.; Neithamer, D. R.; Sun, L. S.; Hetzner, J. E.; Hilty, S.; Hong, S.; Krause, M.; Beyerlein, K. High-Throughput Analysis in Catalysis Research Using Novel Approaches to Transmission Infrared Spectroscopy. *J. Comb. Chem.* **2003**, *5*, 238−244.

(3) Khalafi-Nezhad, A.; Mohammadi, S. Magnetic, Acidic, Ionic Liquid-Catalyzed One-Pot Synthesis of Spirooxindoles. *ACS Comb. Sci.* **2013**, *15*, 512−518.

(4) Zou, Z.; Liu, Y.; Li, H.; Liao, Y.; Xie, C. Synthesis of TiO_2/WO_3/MnO_2 Composites and High-Throughput Screening for their Photoelectrical Properties. *J. Comb. Chem.* **2010**, *12*, 363−369.

(5) Liao, Y.; Li, H.; Liu, Y.; Zou, Z.; Zeng, D.; Xie, C. Characterization of Photoelectric Properties and Composition Effect of TiO_2/ZnO/Fe_2O_3 Composite by Combinatorial Methodology. *J. Comb. Chem.* **2010**, *12*, 883−889.

(6) Potyrailo, R. A.; Mirsky, V. M. Combinatorial and High-Throughput Development of Sensing Materials: The First 10 Years. *Chem. Rev.* **2008**, *108*, 770−813.

(7) Semancik, S.; Cavicchi, R. E.; DeVoe, D. L.; McAvoy, T. J. *Correlation of Chemisorption and Electronic Effects for Metal Oxide Interfaces: Transducing Principles for Temperature Programmed Gas Microsensors*; National Institute of Standards and Technology (US): Gaithersburg, MD, 2001

(8) Simon, U.; Sanders, D.; Jockel, J.; Heppel, C.; Brinz, T. Design Strategies for Multielectrode Arrays Applicable for High-Throughput Impedance Spectroscopy On Novel Gas Sensor Materials. *J. Comb. Chem.* **2002**, *4*, 511−515.

(9) Sanders, D.; Simon, U. High-Throughput Gas Sensing Screening of Surface-Doped In_2O_3. *J. Comb. Chem.* **2007**, *9*, 53−61.

(10) Simon, U.; Sanders, D.; Jockel, J.; Brinz, T. Setup for High-Throughput Impedance Screening of Gas-Sensing Materials. *J. Comb. Chem.* **2005**, *7*, 682−687.

(11) Zhang, G.; Zhang, S.; Yang, L.; Zou, Z.; Zeng, D.; Xie, C. La_2O_3-Sensitized SnO_2 Nanocrystalline Porous Film Gas Sensors and Sensing Mechanism Toward Formaldehyde. *Sens. Actuators B* **2013**, *188*, 137−146.

(12) Korotcenkov, G. Metal Oxides for Solid-State Gas Sensors: What Determines Our Choice? *Mater. Sci. Eng. B* **2007**, *139*, 1−23.

(13) Xie, C.; Xiao, L.; Hu, M.; Bai, Z.; Xia, X.; Zeng, D. Fabrication and Formaldehyde Gas-Sensing Property of ZnO−MnO_2 Coplanar Gas Sensor Arrays. *Sens. Actuators B* **2010**, *145*, 457−463.

(14) Tian, S.; Yang, F.; Zeng, D.; Xie, C. Solution-Processed Gas Sensors Based On ZnO Nanorods Array with an Exposed (0001) Facet for Enhanced Gas-Sensing Properties. *J. Phys. Chem. C* **2012**, *116*, 10586−10591.

(15) Ge, C.; Xie, C.; Hu, M.; Gui, Y.; Bai, Z.; Zeng, D. Structural Characteristics and UV-light Enhanced Gas Sensitivity of La-doped ZnO Nanoparticles. *Mater. Sci. Eng. B* **2007**, *141*, 43−48.

(16) Miller, J. B.; Siddiqui, H. R.; Gates, S. M.; Russell, J. N., Jr; Yates, J. T., Jr; Tully, J. C.; Cardillo, M. J. Extraction of Kinetic Parameters in Temperature Programmed Desorption: A Comparison of Methods. *J. Chem. phys.* **1987**, *87*, 6725.

(17) Falconer, J. L.; Schwarz, J. A. Temperature-Programmed Desorption and Reaction: Applications to Supported Catalysts. *Catal. Rev.* **1983**, *25*, 141−227.

(18) Broido, A. A Simple, Sensitive Graphical Method of Treating Thermogravimetric Analysis Data. *J. Polym. Sci., Polym. Phys.* **1969**, *7*, 1761−1773.

(19) Piloyan, G. O.; Ryabchikov, I. D.; Novikova, O. S. Determination of Activation Energies of Chemical Reactions by Differential Thermal Analysis. *Nature* **1966**, *122*, 1229.

(20) Seiyama, T.; Kato, A.; Fujiishi, K.; Nagatani, M. A New Detector for Gaseous Components Using Semiconductive Thin Films. *Anal. Chem.* **1962**, *34*, 1502−1503.

(21) Yildiz, A.; Serin, T.; Öztürk, E.; Serin, N. Barrier-Controlled Electron Transport in Sn-doped ZnO Polycrystalline Thin Films. *Thin Solid Films* **2012**, *522*, 90−94.

(22) Yamazoe, N.; Shimanoe, K.; Sawada, C. Contribution of Electron Tunneling Transport in Semiconductor Gas Sensor. *Thin Solid Films* **2007**, *515*, 8302−8309.

(23) McAleer, J. F.; Moseley, P. T.; Norris, J. O.; Williams, D. E. Tin Dioxide Gas Sensors. Part 1. Aspects of the Surface Chemistry Revealed by Electrical Conductance Variations. *J. Chem. Soc., Faraday Trans. 1* **1987**, *83*, 1323−1346.

(24) Ding, X.; Zeng, D.; Xie, C. Controlled Growth of SnO_2 Nanorods Clusters Via Zn Doping and its Influence On Gas-Sensing Properties. *Sens. Actuators B* **2010**, *149*, 336−344.

(25) Cui, Z.; Liu, J.; Zeng, D.; Liu, H.; Xie, C. Quasi-One-Dimensional Bismuth Tungsten Oxide Nanostructures Templated by Cotton Fibers. *J. Am. Ceram. Soc.* **2010**, *93*, 1479−1483.

(26) Yu, X.; Meng, D.; Liu, C.; He, X.; Wang, Y.; Xie, J. Structure and Ferromagnetism of Fe-Doped and Fe- and Co-Codoped ZnO Nanoparticles Synthesized by Homogeneous Precipitation Method. *Mater. Lett.* **2012**, *86*, 112−114.

(27) Francioso, L.; Forleo, A.; Capone, S.; Epifani, M.; Taurino, A. M.; Siciliano, P. Nanostructured In_2O_3-SnO_2 Sol−Gel Thin Film as Material for NO_2 Detection. *Sens. Actuators B* **2006**, *114*, 646−655.

(28) J Willett, M.; N Burganos, V.; D Tsakiroglou, C.; C Payatakes, A. Gas Sensing and Structural Properties of Variously Pretreated Nanopowder Tin (IV) Oxide Samples. *Sens. Actuators B* **1998**, *53*, 76−90.

(29) Chen, M.; Wang, Z.; Han, D.; Gu, F.; Guo, G. Porous ZnO Polygonal Nanoflakes: Synthesis, Use in High-Sensitivity NO_2 Gas Sensor, and Proposed Mechanism of Gas Sensing. *J. Phys. Chem. C* **2011**, *115*, 12763−12773.

(30) Li, J.; Liu, Y.; Zhu, Z.; Zhang, G.; Zou, T.; Zou, Z.; Zhang, S.; Zeng, D.; Xie, C. A Full-Sunlight-Driven Photocatalyst with Super Long-Persistent Energy Storage Ability. *Sci. Rep.* **2013**, *3*.

(31) Kılıç, Ç.; Zunger, A. Origins of Coexistence of Conductivity and Transparency in SnO_2. *Phys. Rev. Lett.* **2002**, *88*, No. 095501.

(32) Ho, C.; Chan, C.; Tien, L.; Huang, Y. Direct Optical Observation of Band-Edge Excitons, Band Gap, and Fermi Level in Degenerate Semiconducting Oxide Nanowires In_2O_3. *J. Phys. Chem. C* **2011**, *115*, 25088−25096.